



# Myocardial blood flow quantitation in patients with congestive heart failure: head-to-head comparison between rapid-rotating gantry SPECT and CZT SPECT

Rongzheng Ma, MD,<sup>a</sup> Lei Wang, MD, PhD,<sup>a</sup> Dayong Wu, MD,<sup>a</sup> Meng Wang, MD,<sup>a</sup> Xiaoxin Sun, MD,<sup>a</sup> Bailing Hsu, PhD,<sup>b,c</sup> and Wei Fang, MD<sup>a</sup>

<sup>a</sup> Department of Nuclear Medicine, Fuwai Hospital, National Center for Cardiovascular Diseases, Chinese Academy of Medical Sciences and Peking Union Medical College, Beijing, China

<sup>b</sup> Nuclear Science and Engineering Institute, University of Missouri-Columbia, Columbia, MO

<sup>c</sup> Department of Biomedical Imaging and Radiological Sciences, National Yang-Ming University, Taipei, Taiwan

Received Nov 22, 2018; accepted Jan 1, 2019

doi:10.1007/s12350-019-01621-2

**Purpose.** Recently, the feasibility of myocardial blood flow (MBF) quantitation using rapid-rotating gantry (RRG) and cadmium–zinc–telluride (CZT) SPECT cameras has been demonstrated. We compared MBF quantitation using these two camera systems.

**Methods.** Twenty patients with congestive heart failure (CHF) and 20 patients without CHF (non-CHF) were included. On two consecutive days, dynamic SPECT imaging was performed after a bolus injection of 20 mCi of <sup>99m</sup>Tc-Sestamibi (MIBI) with RRG-SPECT and list-mode acquisition with CZT-SPECT. All dynamic SPECT images were reconstructed with full physical corrections, corrections for ventricular spillover and partial volume effect, using one-tissue kinetic modeling. Resting MBF converted from K1 was then corrected for MIBI extraction fraction and adjusted for rate-pressure product.

**Results.** In both patient groups, there was no significant difference between resting MBF values measured with RRG-SPECT and CZT-SPECT systems ( $P = 0.06$ ,  $P = 0.2$  respectively). For CHF patients, linear regression (LR) was  $y(\text{RRG}) = 1.0412x$  (CZT) ( $r = 0.97$ ) with a small systemic difference ( $\Delta = 0.03 \text{ mL}\cdot\text{min}^{-1}\cdot\text{g}^{-1}$ , 95% CI  $-0.11$  to  $0.20$ ) by Bland–Altman analysis. For non-CHF patients, LR was  $y(\text{RRG}) = 1.025x$  (CZT) ( $r = 0.89$ ) with also small systemic difference ( $\Delta T = 0.02 \text{ mL}\cdot\text{min}^{-1}\cdot\text{g}^{-1}$ , 95% CI  $-0.14$  to  $0.19$ ) in BA analysis.

**Conclusion.** Physical corrections along with other image corrections can provide comparable MBF quantitations in both CHF and non-CHF patients, regardless of the type of SPECT systems used. (J Nucl Cardiol 2020;27:2287–302.)

**Key Words:** SPECT myocardial blood flow quantitation • rapid-rotating SPECT • CZT SPECT • congestive heart failure • physical corrections • corrections of left and right ventricle spillovers • correction of <sup>99m</sup>Tc-Sestamibi extraction fraction

**Electronic supplementary material** The online version of this article (<https://doi.org/10.1007/s12350-019-01621-2>) contains supplementary material, which is available to authorized users.

The authors of this article have provided a PowerPoint file, available for download at SpringerLink, which summarises the contents of the paper and is free for re-use at meetings and presentations. Search for the article DOI on SpringerLink.com.

Rongzheng Ma and Lei Wang have contributed equally to this work.

**Funding** This research was supported by a grant from National Natural Science Foundation of China (Grant No.: 81771872).

Reprint requests: Wei Fang, MD, Xiaoxin Sun, MD, Department of Nuclear Medicine, Fuwai Hospital, National Center for Cardiovascular Diseases, Chinese Academy of Medical Sciences and Peking Union Medical College, 167 Beilishi Road, Beijing 100037, China; [nuclearfw@126.com](mailto:nuclearfw@126.com), [xxsunfw@126.com](mailto:xxsunfw@126.com) and Bailing Hsu, PhD, Nuclear Science and Engineering Institute, University of Missouri-Columbia, E2433 Lafferre Hall, Columbia, MO 65211, USA; [bailingshu@gmail.com](mailto:bailingshu@gmail.com)  
1071-3581/\$34.00

Copyright © 2019 American Society of Nuclear Cardiology.

**Abbreviations**

SPECT	Single photon emission computed tomography
RRG	Rapid-rotating gantry
CZT	Cadmium–zinc–telluride
MBF	Myocardial blood flow
CHF	Congestive heart failure
MIBI	<sup>99m</sup> Tc-Sestamibi
ESV	End-systolic volume
EDV	End-diastolic volume
FBV	Fractional blood volume
RPC	Repeatability coefficient

**See related editorial, pp. 2303–2305**

**INTRODUCTION**

Recent advances in single photon emission computed tomography (SPECT) imaging technology, such as novel gantry designs, solid-state detectors, and innovative collimation, created imaging devices with markedly improved temporal resolution and sensitivity, which allow for dynamic SPECT imaging. Several investigators explored the feasibility of quantitating regional myocardial blood flow (MBF) using <sup>99m</sup>Tc-labeled myocardial perfusion tracers, and these state-of-the-art dynamic SPECT cameras.<sup>1–8</sup> So far, two types of gamma cameras have been fully investigated: conventional dual-headed SPECT camera equipped with a rapid rotational gantry and parallel-hole collimation (RRG-SPECT)<sup>1,2,5,6</sup>; and cadmium-zinc-telluride (CZT) SPECT camera with stationary gantry and multipinhole or parallel-hole collimation.<sup>3,4,7,8</sup> Each camera design provides unique imaging characteristics for MBF quantitation. The RRG-SPECT camera with the capability of rapid back-and-forth gantry rotation enables dynamic SPECT acquisition to measure arterial input function of radiotracer in myocardium. The CZT-SPECT camera with solid-state detectors and a fixed gantry design, has the additional advantage of increased energy resolution and count sensitivity, which makes this camera well suited for dynamic SPECT imaging with list-mode data acquisition.<sup>9,10</sup> However, it has been reported that the accuracy of quantitative regional MBF with SPECT cameras can be significantly affected by multiple factors such as tissue attenuation, image noise, image resolution, scattered photons, patient motion, and low myocardial radiotracer extraction.<sup>4,6,7</sup> While MBF quantitation with positron emission tomography serves as the gold standard, MBF quantitation with dynamic SPECT may approach positron emission tomography MBF quantitation if these factors in the process of MBF quantitation can be fully addressed.<sup>6,7</sup> In the present study, we performed a head-to-head comparison of

measured resting MBF values of patients with congestive heart failure (CHF) and non-CHF patients using RRG-SPECT and CZT-SPECT cameras, reconstructed with implementation of full physical image corrections.

**METHODS****Study Population**

Twenty clinically stable CHF patients with mild-to-severe chronic left ventricular dysfunction (LVEF < 50%) by echocardiography were included. In this group, 19 of 20 patients were clinically diagnosed as ischemic cardiomyopathy on the basis of clinical evidence that coronary artery disease was most likely the cause of left ventricular dysfunction. Their symptoms (> 3 months) were graded according to the New York Heart Association functional classification (I to IV). Characteristics of the study subjects are shown in Table 1. The comparison group consisted of 20 patients with preserved LVEF (≥ 50%) by echocardiography, who were suspected of having coronary artery disease. This group will be referred to as “non-CHF” group.

All participants gave written informed consent, approved by the institutional Research Ethics Board of Fuwai Hospital, Beijing, China.

**Imaging Equipment**

Dynamic SPECT imaging was performed using two cameras: a RRG-SPECT scanner with integrated CT (RRG-SPECT/CT) camera (Symbia T16, Siemens, USA) and a multipinhole CZT-SPECT camera (Discovery NM 530c, GE, USA). The SPECT component of the RRG-SPECT/CT camera is equipped with a 0.95 cm NaI(Tl) scintillation crystal and low-energy high-resolution collimation. Using this camera, resting dynamic SPECT imaging was performed with 18 dynamic frames and 1152 projections, with 18 back-and-forth rotations of the gantry traversing an arc of 180° with a total acquisition time of 10 min (ten 10 seconds, five 20 seconds, two 60 seconds, and one 280 seconds acquisitions). Other relevant imaging parameters were continuous gantry motion, circular orbit, 64×64 matrix, 1.78 zoom factor, 5.39 mm pixel size, and two energy windows positioned over the <sup>99m</sup>Tc photopeak (126 to 154 keV) and scatter counts (109 to 125 keV). The CZT SPECT camera was equipped with 19 CZT detector panels, composed of four 5-mm-thick elements with 32 × 32 pixels and an 180° arc of focused pinhole collimators (effective diameter = 5.1 mm) with the capability to perform list-mode data acquisition.<sup>9</sup> Resting dynamic SPECT imaging with the CZT-SPECT camera was performed in list-mode for 10 min and then rebinned to generate 18 matched dynamic frames (ten 10 seconds, five 20 seconds, two 60 seconds, and one 280 seconds acquisitions). Other relevant imaging parameters were 32 × 32 matrix, 2.46 mm pixel size, and two energy windows over the <sup>99m</sup>Tc photopeak (131.6 to 148.4 keV), and scatter photons (118.4 to 131.5 keV). For attenuation

**Table 1.** Characteristics of study patients

Characteristics	CHF (N = 20)	Non-CHF (N = 20)
Age	60 ± 10 <sup>a</sup> (33 to 73 <sup>b</sup> )	55 ± 9 <sup>a</sup> (35 to 77 <sup>b</sup> )
Male	17 (85%)	12 (60%)
Body mass index	23 ± 3 <sup>a</sup> (19 to 23 <sup>b</sup> )	24 ± 3 <sup>a</sup> (20 to 30 <sup>b</sup> )
Echo LVEF	37 ± 5% <sup>a</sup> (29 to 49% <sup>b</sup> )	*64 ± 5% <sup>a</sup> (54–72% <sup>b</sup> )
NYHA class I	5 (25%)	20 (100%)
NYHA class II	6 (30%)	-
NYHA class III	8 (40%)	-
NYHA class IV	1 (5%)	-
Hypertension	13 (65%)	9 (45%)
Hyperlipidemia	15 (75%)	12 (60%)
Diabetes mellitus	13 (65%)	5 (25%)
Tobacco use	11 (55%)	6 (30%)
Family history of CAD	8 (40%)	5 (25%)
Dyspnea	8 (40%)	15 (75%)
Atypical chest tightness	15 (75%)	8 (40%)
Angina	19 (95%)	2 (10%)
Prior PCI	10 (50%)	-
Prior CABG	3 (15%)	-
Prior MI	13 (63%)	-
Ischemic cardiomyopathy	19 (95%)	-

CHF, congestive heart failure; NYHA, New York Heart Association functional class; LVEF, left ventricular ejection fraction; CAD, coronary artery disease; PCI, percutaneous coronary intervention; CABG, coronary artery bypass grafting; MI, myocardial infarction

<sup>a</sup>Mean ± SD

<sup>b</sup>Range

\**P* < 0.05

correction, a low-dose CT scan (120 keV, 30 mAs, 5.2 seconds) was performed by the RRG-SPECT/CT camera after dynamic SPECT acquisition was completed. The attenuation correction map was then used for attenuation correction of both RRG-SPECT and CZT-SPECT dynamic image data.

### Imaging Protocol

All patients underwent resting dynamic SPECT imaging with RRG-SPECT/CT camera first, followed by CZT-SPECT imaging on two consecutive days. These patients were, as much as possible, placed in precisely the same position under both cameras. Before imaging, all patients drank 300 to 500 mL of water to reduce spillover from adjacent MIBI liver activity and were asked to remain in relaxed supine position for recording baseline heart rate and blood pressure. With both arms raised over the head, dynamic SPECT imaging was started, followed by administering an intravenous bolus injection of 20 mCi of <sup>99m</sup>Tc-Sestamibi (MIBI) 10 seconds later. To verify correct patient positioning for CZT-SPECT, a pilot injection of 1.0 mCi of MIBI was given prior to dynamic imaging. Sixty minutes after completion of dynamic SPECT imaging, conventional ECG-gated SPECT imaging was performed.

### Myocardial Counts and Count Rate

Dynamic SPECT images were initially reconstructed using filtered back projection and summed to create static images from the last three dynamic frames (200–600 seconds). Patient-specific volumes of interest were manually drawn on summed images to only include the myocardial region and to create a set of 2D masks by forward projecting the volume of interest to corresponded angles (e.g., 64 and 19 angles in 180° arc for RRG-SPECT and CZT-SPECT, respectively). The 2D masks were used to automatically localize myocardial regions in the dynamic projection data to measure frame-specific total thousand counts (kcts) and record count rate in thousand counts per second (kcps).

### Dynamic Image Reconstruction

The dynamic projection data of RRG-SPECT were precorrected for <sup>99m</sup>Tc isotope decay, and reconstructed by ordered subsets expectation maximization (6 iterations, 8 subsets) with full physical corrections for photon attenuation and scatter, collimator resolution, and Poisson count-statistics as described previously.<sup>2,6,11–16</sup> In addition, angular inconsistency due to rapidly changing biodistribution of MIBI activity into the SPECT field-of-view was corrected by compensating

photon counts in empty angles using back-projection and forward-projection of those angles with photon counts. Prior to dynamic image reconstruction, the co-registration of initial filtered back projection SPECT and CT images was verified visually and manually corrected for misregistration by applying 3D translation. Image reconstruction for CZT-SPECT data was similar to that for RRG-SPECT. Initially, projections rebinned from list-mode data were precorrected for  $^{99m}\text{Tc}$  isotope decay. The scatter was estimated using a low-energy window (118.4 to 131.5 keV) and subtracted from the  $^{99m}\text{Tc}$  photopeak (131.6 to 148.4 keV) counts. Dynamic SPECT

images were reconstructed by ordered subsets expectation maximization (35 iterations, 2 subsets) using a system matrix to model the geometry of each pinhole and detector panel relative to the image center. Pinhole collimator resolution recovery was performed in the forward-projection step of ordered subsets expectation maximization by modeling each pinhole as a small disk that was radially sampled by 21 rays, starting from each detector element to account for the image blurring due to the limited physical size of pinhole.<sup>17</sup> Noise reduction was achieved by statistical modeling of Poisson noise in the reconstruction process.<sup>15,16</sup>

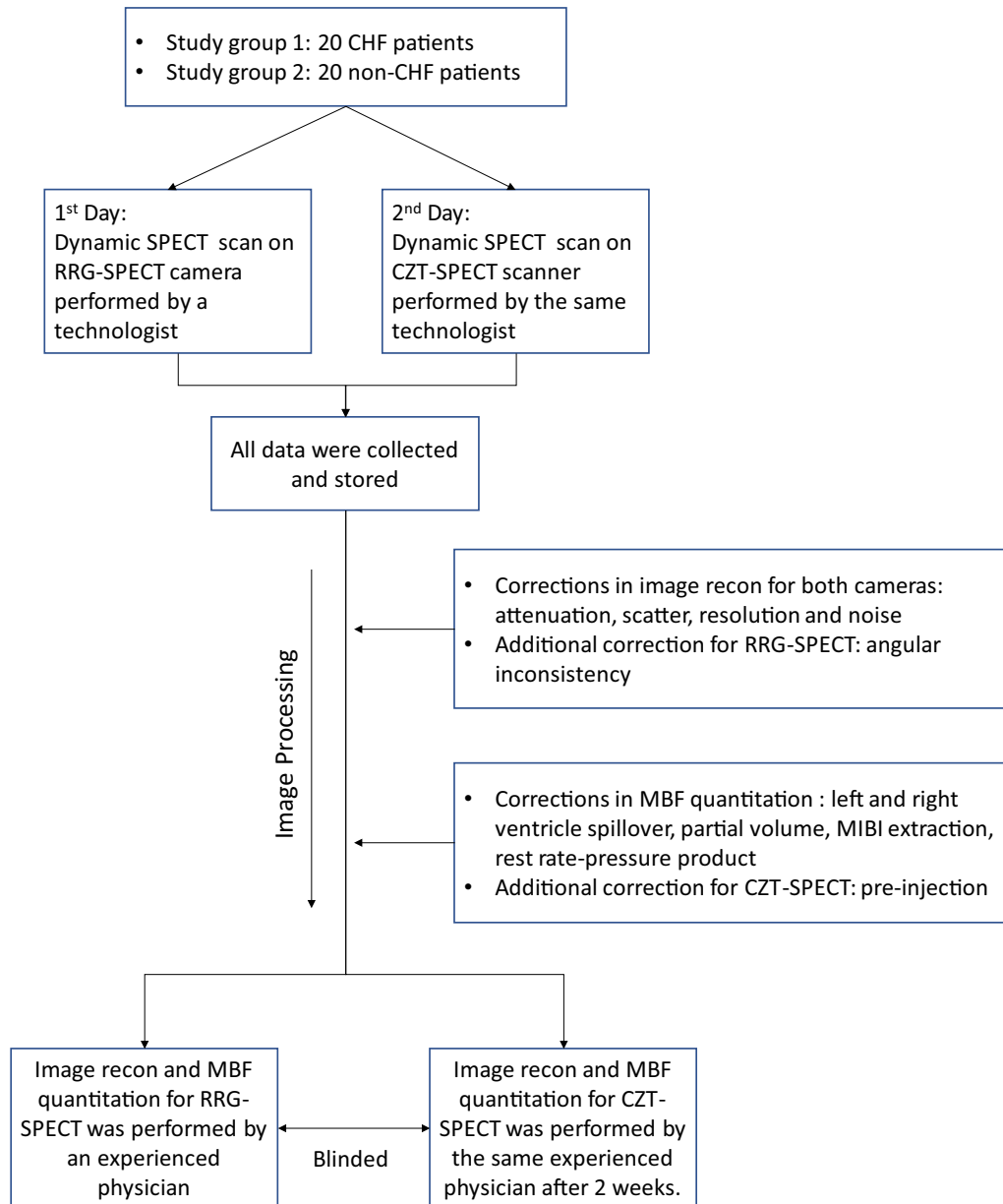


**Figure 1.** A flowchart of study design.

### SPECT MBF Quantitation

To quantitate resting MBF values, the dynamic SPECT images were manually reoriented in the short-axis view. The myocardial centerline contour was automatically detected using ellipsoid-approximated geometry. The mitral valve plane was manually determined from static images, created by summing the last three frames of dynamic short-axis images (from 200 to 600 seconds). A MIBI myocardial time-activity curve was generated by placing the myocardial centerline over all dynamic frames, and from these data, dynamic polar maps of resting MBF were generated. The arterial input function time-activity curve was created automatically by placing a rectangular volume of interest (10x10x40 mm) over left ventricular regions and atrium with 1:2 volume ratio and manually adjusted when needed. A one-tissue compartment (two-compartment) kinetic model was implemented for MIBI tracer to fit three kinetic parameters by numeric optimization using the Levenberg–Marquardt method, including (K1, k2) transport coefficients, fractional blood volume (FBV) for blood-pool spillover estimation, and (1-FBV) for partial volume correction to myocardial uptake as follows<sup>18</sup>:

$$C_{myo}(t) = FBV \cdot C_a(t) + (1 - FBV) \cdot K_1 e^{-k_2 t} \otimes C_a(t),$$

where  $C_{myo}(t)$  and  $C_a(t)$  are the measured activity concentrations in myocardium and blood-pool for arterial input obtained from dynamic SPECT images, respectively. Prior to the kinetic modeling, the dynamic polar map from the early frame of myocardium before the incoming MIBI activity into the left heart region was analyzed with two volumes of interest placed in septal and lateral walls, respectively. Activity renormalization in septal wall region was performed by the threshold of activity in the lateral wall region to correct for the right ventricle spillover. In addition, for CZT-SPECT, residual activity in myocardium from the preinjection localization scan was estimated from the first frame and subtracted for the subsequent frames.

For both RRG-SPECT and CZT-SPECT, whole-left ventricle (global) K1, k2, and FBV were first fitted from the global myocardial and arterial input time-activity curves. The one-tissue kinetic model was then modified by introducing a constraint of fixed k2 obtained from the global k2 value before fitting FBV and K1 values in the individual polar map pixels. Resting MBF was estimated from the K1 kinetic parameter by applying the correction for MIBI tracer extraction fraction  $[1 - 0.816 \times \exp(-0.267/MBF)]$  as determined from a previous comparative study of MIBI and positron emission tomography <sup>13</sup>N-Ammonia tracers.<sup>6</sup> To compensate for physiological variance, resting MBF was adjusted for the baseline heart rate and systolic blood pressure by a factor of rate-pressure product divided by 10000.<sup>19</sup> MBF was then quantitated with a unit of (mL·min<sup>-1</sup>·g<sup>-1</sup>). Resting global and regional MBF values were displayed in polar maps, showing regional MBF in three coronary territories.

**Table 2.** Hemodynamic data of CHF and non-CHF patients

	CHF		Non-CHF	
	RRG-SPECT	CZT-SPECT	RRG-SPECT	CZT-SPECT
Hemodynamics				
Heart rate (bpm)	81 ± 19 (45 to 122)	76 ± 16 (50 to 102)	77 ± 13 (51 to 103)	81 ± 16.0 (54 to 108)
Systolic BP (mmHg)	113 ± 19 (84 to 170)	115 ± 21 (118; 83 to 163)	128 ± 13 (106 to 151)	130 ± 18 (93 to 174)
Diastolic BP (mmHg)	76 ± 11 (60 to 95)	76 ± 10 (60 to 96)	85 ± 9.0 (73 to 111)	86 ± 12 (72 to 118)
RPP (bpm × mmHg)	9162 ± 2822 (4956 to 15,980)	8702 ± 2463 (5561 to 14,670)	9907 ± 2096 (6996 to 14,420)	10,588 ± 2998 (6138 to 18,792)

Hemodynamic data were recorded immediately before dynamic imaging with RRG-SPECT and CZT-SPECT systems  
Bpm, beats per minute; BP, blood pressure; RPP, rate-pressure product

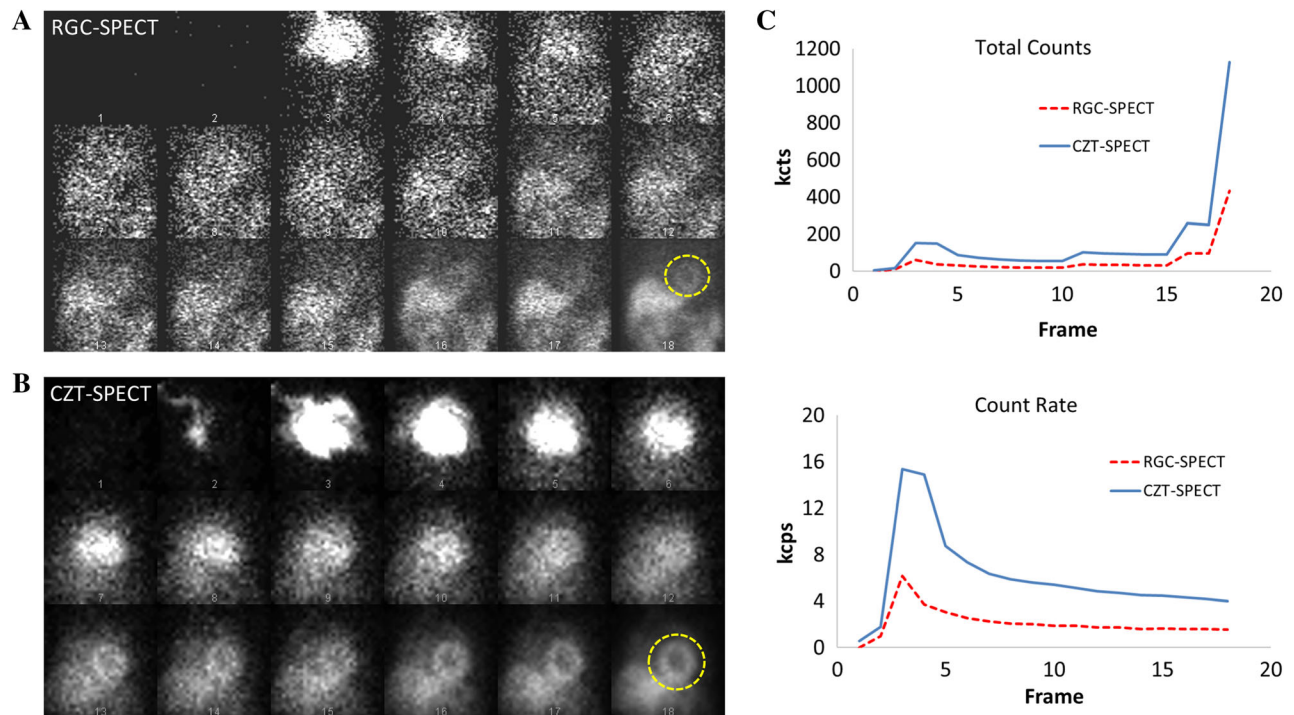


**Figure 2.** Example of dynamic SPECT acquisition in a patient with LV dysfunction. (A) 18 frames of dynamic projection images in the anterior view using the RRG-SPECT camera are shown. The bolus injection of MIBI was given 10 s after start of imaging (frame 2); (B) 18 frames of dynamic projection images in the anterior view with the CZT-SPECT camera. The yellow circle in A and B is the angular-dependent 2D mask to include only the myocardium in all dynamic frames. Total counts and count rate are derived from this volume of interest (VOI). (C) Time activity curve from the VOI, providing total counts (thousand counts, kcts) and count rate (thousand counts per second, kcps) using the RRG-SPECT and CZT-SPECT, respectively. The higher count rate with CZT-SPECT can be appreciated.

### Test-Retest Reproducibility

In this study, reconstructions and analyses of RRG-SPECT and CZT-SPECT image data were performed using a cardiac software package (MyoFlowQ, Taiwan). This software incorporates image reconstruction and MBF flow processing on a single platform to generate quantitative MBF information. This software is capable of reconstructing rest and stress dynamic SPECT images simultaneously as the reconstruction work can be accomplished in 15 minutes. The program is highly automated, and designed to allow a user to adjust angles and center of image reorientation to generate short-axis slices and adjust the location of blood-pool box when necessary. The processing time to generate the result of MBF quantitation would normally take another 12 to 15 minutes. To assess test-retest reproducibility of quantitating MBF by two image acquisitions performed by the same experienced technologist on RRG-SPECT and CZT-SPECT cameras, and subsequent image processing performed by the same experienced physician for CHF and non-CHF groups, resting MBF of 20 CHF

and non-CHF patients was analyzed separately to calculate mean resting MBF of both cameras and the corresponded repeatability coefficient that was further presented as a percentage of mean resting MBF. When working on the image processing, the experienced physician was blinded to patient's clinical information. When working on the processing for CZT-SPECT, the experienced physician was blinded to the result of the first processing of RRG-SPECT as two analyses were taken 2 weeks apart. The flowchart of study design is shown in Figure 1.

### Assessment of Myocardial Perfusion Defect and Left Ventricular Function

Conventional MIBI myocardial perfusion and ECG-gated images were reconstructed and processed using commercially available software (QPS/QGS, Cedar-Sinai Medical Center, Los Angeles, USA). Myocardial perfusion defects were quantitated using a 17-segment model. Segmental myocardial

**Table 3.** Mean total counts and count rate within myocardial VOI in 18 dynamic frames acquired with RRG-SPECT and CZT-SPECT in all 40 study patients after a bolus injection of 20 mCi of MIBI

Dynamic frame	Frame duration (s)	RRG-SPECT				CZT-SPECT			
		Total counts (kcts)		Count rate (kcps)		Total counts (kcts)		Count rate (kcps)	
		Mean	SD	Mean	SD	Mean	SD	Mean	SD
1	10	0.0	0.0	0.00	0.00	16.5	6.0	1.65	0.60
2	10	12.2	18.6	1.22	1.86	34.4	22.3	3.44	2.23
3	10	87.0	40.2	8.70	4.02	207.1	145.8	20.71	14.58
4	10	101.5	45.2	10.15	4.52	308.8	139.1	30.87	13.91
5	10	79.1	42.4	7.91	4.24	273.9	91.9	27.39	9.19
6	10	68.1	34.0	6.80	3.40	234.9	81.0	23.49	8.10
7	10	61.1	28.6	6.11	2.85	213.9	79.6	21.39	7.96
8	10	56.6	24.4	5.66	2.44	195.3	72.0	19.53	7.20
9	10	52.2	22.4	5.22	2.24	178.2	58.0	17.82	5.80
10	10	49.4	20.5	4.93	2.05	166.5	49.8	16.65	4.98
11	20	93.5	39.0	4.67	1.95	309.8	88.5	15.49	4.42
12	20	88.7	36.8	4.43	1.84	288.1	78.8	14.41	3.94
13	20	85.6	35.0	4.28	1.75	273.4	72.0	13.67	3.60
14	20	83.3	34.2	4.17	1.71	262.7	68.6	13.14	3.43
15	20	81.8	33.6	4.09	1.68	254.7	65.2	12.73	3.26
16	60	238.1	95.1	3.97	1.58	728.7	181.6	12.15	3.03
17	60	231.9	92.0	3.87	1.53	697.5	170.6	11.62	2.84
18	280	1037.8	404.4	3.71	1.44	3070.3	730.5	10.97	2.61

*Kcts*, thousand counts; *kcps*, thousand counts per second  
 The counts in the first frame of the CZT camera are due to the pilot MIBI injection, prior to start of dynamic imaging

perfusion defect scores and total summed rest score were automatically generated relative to a normal database. Functional left ventricular parameters, such as end-systolic volume (ESV), end-diastolic volume (EDV), and LVEF were also computed by the same software.

**Statistical Analysis**

Noncontinuous variables, such as patient characteristics were expressed as number and percentage. Continuous variables were expressed as mean ± standard deviation and range. Differences of mean values for the CHF and non-CHF group were tested by multiple factor ANOVA (with interactions). Resting MBF values, quantitated from RRG-SPECT and CZT SPECT, for both CHF and non-CHF groups, were compared by linear regression, and systematic differences were analyzed by Bland-Altman plot. RPC values representing test-retest

repeatability of resting MBF between RRG-SPECT and CZT-SPECT for both CHF and non-CHF groups were calculated as per formula:  $RPC = 1.96 \times \text{standard deviation of difference between the two measurements}$ .<sup>1</sup> Percentage as  $RPC / (\text{mean resting MBF}) \times 100\%$  was determined to assess the level of RPC while normalized to mean resting MBF for CHF and non-CHF groups. A p-value < 0.05 was considered statistically significant.

**RESULTS**

Resting hemodynamics prior to dynamic image acquisition using RRG-SPECT and CZT-SPECT cameras are shown in Table 2. There were no significant differences ( $P = 0.15$ ) in resting heart rate and resting rate-pressure product between CHF and non-CHF patients while imaging using both the cameras.

**Table 4.** Global and regional resting MBF in 20 CHF patients and 20 non-CHF patients quantitated by RRG-SPECT and CZT-SPECT

#	CHF										Non-CHF									
	RRG-SPECT					CZT-SPECT					RRG-SPECT					CZT-SPECT				
	LV	LAD	LCX	RCA	LV	LAD	LCX	RCA	LV	LAD	LCX	RCA	LV	LAD	LCX	RCA	LV	LAD	LCX	RCA
1	0.49	0.34	0.61	0.58	0.5	0.36	0.47	0.71	0.73	0.67	0.73	0.79	0.84	0.89	0.71	0.90	0.90	0.90	0.90	0.90
2	1.08	1.03	1.09	1.12	0.87	0.99	0.82	0.76	1.33	1.32	1.18	1.3	1.25	1.26	1.26	1.23	1.23	1.23	1.23	1.23
3	0.63	0.62	0.77	0.49	0.65	0.76	0.64	0.49	1.06	1.04	1.05	1.1	1.02	0.99	1.02	1.06	1.06	1.06	1.06	1.06
4	0.93	0.96	0.95	0.86	0.90	0.98	0.87	0.81	0.98	0.95	1.02	0.98	1.02	1.03	1.09	0.93	0.93	0.93	0.93	0.93
5	0.89	1.14	0.93	0.5	0.95	1.19	0.94	0.64	1.03	1.06	1.04	0.98	0.99	0.94	1.08	0.97	0.97	0.97	0.97	0.97
6	0.43	0.37	0.53	0.4	0.48	0.44	0.49	0.51	1.13	1.1	1.13	1.15	1.23	1.26	1.09	1.33	1.33	1.33	1.33	1.33
7	0.60	0.58	0.70	0.52	0.53	0.53	0.68	0.37	1.35	1.23	1.12	1.53	1.22	1.23	1.11	1.31	1.31	1.31	1.31	1.31
8	1.30	1.29	1.30	1.30	1.27	1.38	1.30	1.08	1.23	1.27	1.19	1.13	1.10	1.11	1.04	1.15	1.15	1.15	1.15	1.15
9	1.07	1.02	1.17	1.06	1.00	1.09	1.04	0.81	1.28	1.3	1.12	1.22	1.11	1.18	1.00	1.10	1.10	1.10	1.10	1.10
10	0.71	0.49	0.97	0.76	0.78	0.62	0.97	0.81	1.40	1.39	1.4	1.43	1.34	1.33	1.38	1.31	1.31	1.31	1.31	1.31
11	1.17	1.22	1.19	1.09	1.04	1.14	1.02	0.93	1.18	1.09	1.04	1.24	1.11	1.18	1.09	1.05	1.05	1.05	1.05	1.05
12	1.01	1.04	0.95	1.01	1.01	1.00	1.05	1.00	1.10	1.08	1.18	1.05	1.16	1.18	1.22	1.08	1.08	1.08	1.08	1.08
13	0.45	0.28	0.58	0.56	0.43	0.25	0.44	0.58	0.98	0.95	0.94	1.06	0.93	0.93	1.00	0.86	0.86	0.86	0.86	0.86
14	0.80	0.71	0.88	0.86	0.76	0.60	0.83	0.92	1.22	1.20	1.27	1.19	1.29	1.36	1.26	1.22	1.22	1.22	1.22	1.22
15	0.48	0.46	0.55	0.43	0.45	0.46	0.50	0.38	1.1	1.07	1.21	1.04	1.16	1.23	0.99	1.25	1.25	1.25	1.25	1.25
16	0.74	0.93	0.49	0.73	0.72	1.06	0.76	0.20	1.19	1.24	1.13	1.19	1.10	1.21	0.96	1.08	1.08	1.08	1.08	1.08
17	0.61	0.59	0.71	0.52	0.53	0.62	0.59	0.34	1.45	1.43	1.46	1.49	1.39	1.34	1.38	1.48	1.48	1.48	1.48	1.48
18	0.54	0.61	0.53	0.50	0.54	0.49	0.64	0.5	0.88	0.82	0.97	0.87	0.91	0.89	0.90	0.94	0.94	0.94	0.94	0.94
19	0.47	0.36	0.58	0.52	0.42	0.35	0.42	0.52	1.00	0.9	1.05	1.09	0.93	0.90	0.91	0.99	0.99	0.99	0.99	0.99
20	0.35	0.19	0.43	0.51	0.35	0.23	0.37	0.49	1.20	1.14	1.26	1.23	1.27	1.27	1.26	1.29	1.29	1.29	1.29	1.29

Unit: mL·min<sup>-1</sup>·g<sup>-1</sup>  
LV, left ventricle; LAD, left anterior descending; left circumflex; RCA, right coronary artery



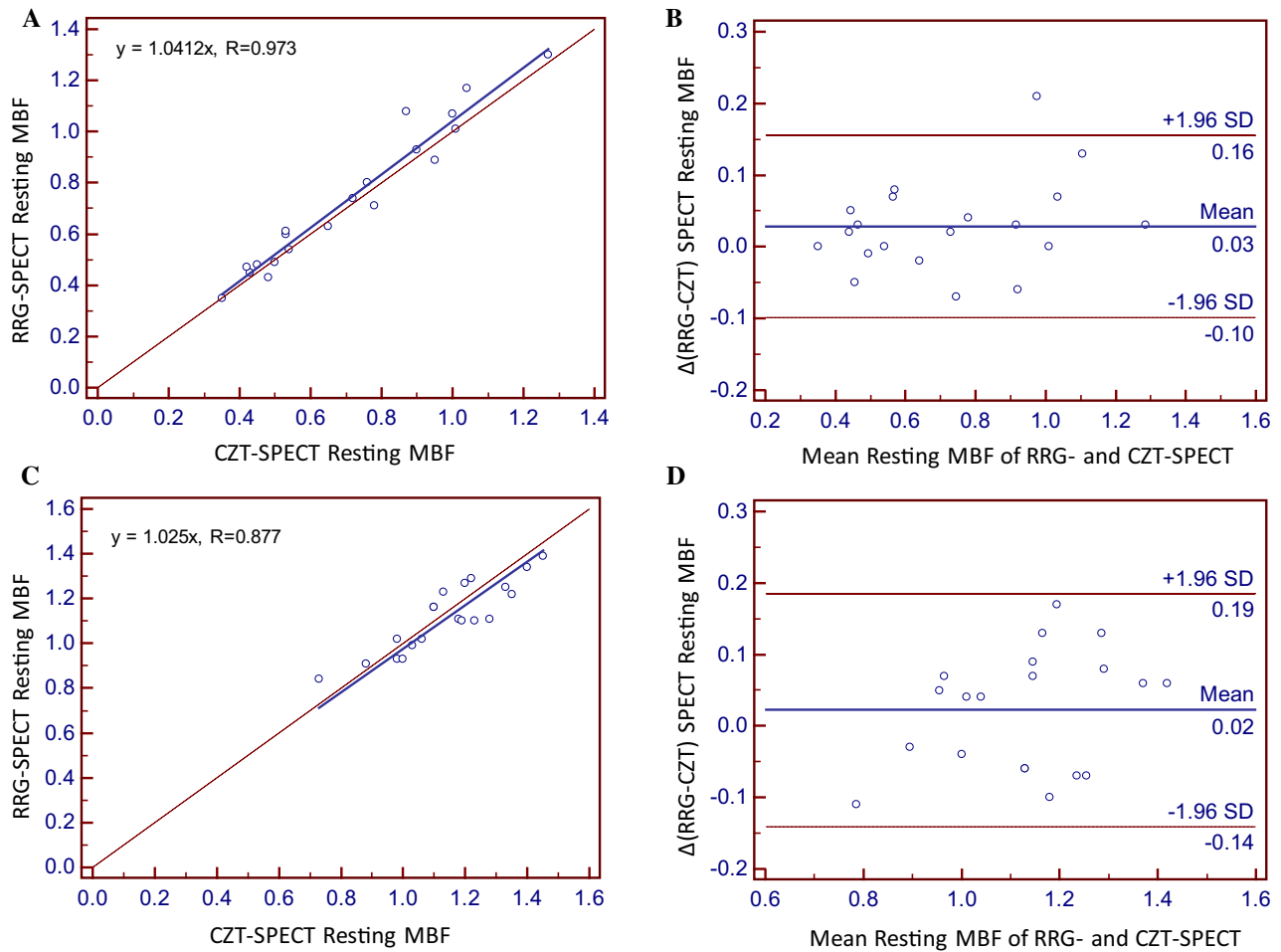


**Figure 3.** Linear regression correlation (A and C) and Bland–Altman plot (B and D) of global resting myocardial blood flow (MBF) quantitated with RRG-SPECT and CZT-SPECT in CHF patients (top panels) and non-CHF patients (bottom panels). MBF is expressed as  $\text{mL}\cdot\text{min}^{-1}\cdot\text{g}^{-1}$ .

### Count Rates

Figure 2 shows examples of serial anterior view projection data acquired by dynamic SPECT imaging using both cameras. When the MIBI bolus reached the left ventricle, mean total counts (kcts) and count rate (kcps) in the myocardial volume of interest were significantly higher with the CZT-SPECT camera than with the RRG-SPECT camera (Table 3, frame 4:  $308 \pm 139$  kcts and  $31 \pm 14$  kcps vs  $102 \pm 45$  and  $10 \pm 5$ ,  $P < 0.0001$ ). Once MIBI had accumulated in the myocardium, count rate (frame 18) had decreased to  $11 \pm 3$  kcps (CZT camera) and  $4 \pm 1$  kcps (RRG camera) (Table 3).

### Myocardial Blood Flow

Table 4 shows calculated resting MBF in individual patients in both groups, after full physical corrections, correction for left ventricle/right ventricle spillover in kinetic modeling, correction for MIBI extraction and rate-pressure product. Overall, non-CHF patients had resting MBF values close to  $1.0 \text{ mL}\cdot\text{min}^{-1}\cdot\text{g}^{-1}$  and were homogeneously distributed over three coronary territories. On the other hand, CHF patients showed lower resting MBF values and were heterogeneously distributed. Linear regression analysis and Bland–Altman plots of global resting MBF obtained with both cameras in individual patients are shown in Figure 3. Over the

**Table 5.** Global and regional resting MBF values in CHF and non-CHF patients imaged with RRG-SPECT and CZT-SPECT camera

	CHF		Non-CHF	
	RRG-SPECT	CZT-SPECT	RRG-SPECT	CZT-SPECT
Resting MBF (mL·min <sup>-1</sup> ·g <sup>-1</sup> )				
Global	0.74 ± 0.28 <sup>&amp;</sup> (0.35 to 1.3)	0.71 ± 0.2 <sup>&amp;</sup> (0.35 to 1.27)	1.14 ± 0.18 (0.73 to 1.45)	1.12 ± 0.15 (0.84 to 1.39)
LAD	0.68 ± 0.37 <sup>&amp;</sup> (0.07 to 1.29)	0.73 ± 0.35 <sup>&amp;</sup> (0.23 to 1.38)	1.11 ± 0.19 (0.67 to 1.46)	1.13 ± 0.16 (0.89 to 1.36)
LCX	0.80 ± 0.29 <sup>&amp;</sup> (0.43 to 1.3)	0.74 ± 0.26 <sup>&amp;</sup> (0.37 to 1.3)	1.12 ± 0.18 (0.73 to 1.46)	1.09 ± 0.16 (0.71 to 1.38)
RCA	0.72 ± 0.27 <sup>&amp;</sup> (0.40 to 1.3)	0.64 ± 0.24 <sup>&amp;</sup> (0.30 to 1.08)	1.15 ± 0.17 (0.79 to 1.53)	1.13 ± 0.15 (0.86 to 1.48)

Data are shown as mean ± SD and range. No significant ( $P > 0.06$ ) differences between RRG-SPECT and CZT-SPECT and CHF and Control group unless otherwise indicated. <sup>&</sup>significant ( $P < 0.0001$ ) difference between CHF and non-CHF groups for RRG-SPECT and CZT-SPECT  
MBF, myocardial blood flow; Global, global MBF; LAD, left anterior descending artery territory; LCX, left circumflex artery territory; RCA, right coronary artery territory

entire range of measured MBF, there was excellent correlation ( $r = 0.97$  in the CHF group and  $r = 0.88$  in the non-CHF group) in measurements between the two camera systems. The Bland–Altman plots show small, but not significant, systematic differences:  $0.03 \text{ mL}\cdot\text{min}^{-1}\cdot\text{g}^{-1}$  in CHF patients and  $0.02 \text{ mL}\cdot\text{min}^{-1}\cdot\text{g}^{-1}$  in non-CHF patients. The limits of agreement were relatively narrow for both patient groups:  $\pm 0.13 \text{ mL}\cdot\text{min}^{-1}\cdot\text{g}^{-1}$  and  $\pm 0.16 \text{ mL}\cdot\text{min}^{-1}\cdot\text{g}^{-1}$ , respectively. Table 5 shows mean global MBF measurements and mean MBF in the three coronary territories (LAD, LCX, and RCA). Mean global MBF was significantly lower in CHF patients than in patients with normal left ventricular function (RRG-SPECT:  $0.74 \pm 0.28$  vs  $1.14 \pm 0.18 \text{ mL}\cdot\text{min}^{-1}\cdot\text{g}^{-1}$ ; CZT-SPECT:  $0.71 \pm 0.2$  vs  $1.12 \pm 0.15$ , all  $P < 0.0001$ ). There was no significant difference ( $P > 0.06$ ) in measurements with either camera. Similarly, mean MBF in each of the coronary artery territories was not significantly different measured with either camera, but in each coronary artery territory MBF was significantly ( $P < 0.0001$ ) lower in patients with left ventricular dysfunction than in patients with normal left ventricular function. Figure 4 shows representative polar maps generated from data acquired with both cameras in a patient with left ventricular dysfunction and a patient of with normal left ventricular function.

The test-retest repeatability of CHF and non-CHF groups imaged with RRG-SPECT and CZT-SPECT, when dynamic imaging was performed by the same experienced technologist and image processing was performed by the same experienced physician, was comparable in 20 CHF patients (RPC =  $0.18 \text{ mL}\cdot\text{min}^{-1}\cdot\text{g}^{-1}$ ) and 20 non-CHF patients ( $0.22 \text{ mL}\cdot\text{min}^{-1}\cdot\text{g}^{-1}$ ), which were equivalent to 25% and 19.2% of their mean resting MBF, respectively (Table 6).

### ECG-Gated Myocardial Perfusion Imaging

Using both SPECT camera systems, CHF patients had significantly larger summed rest score, lower radionuclide LVEF, larger ESV, and larger EDV than non-CHF patients (Table 7, all  $P < 0.0001$ ).

## DISCUSSION

In the present study, quantitative resting MBF values measured, using MIBI by two markedly different dynamic SPECT camera systems, were not statistically different over a wide range of resting MBF values, in two clinically distinctly different patient groups.

We used nearly identical imaging and processing protocols for the two camera systems. In addition, we applied identical physical corrections for image

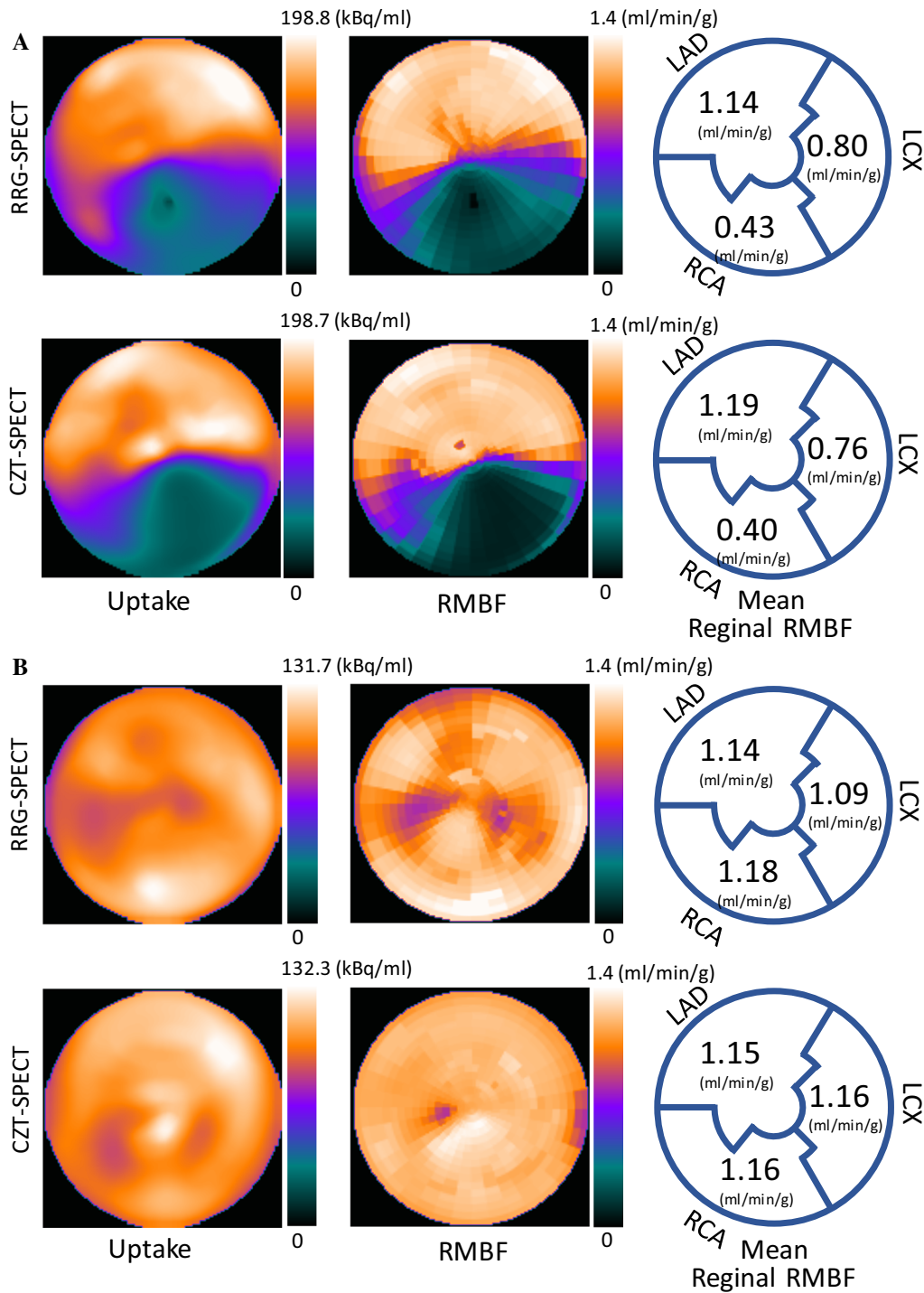


**Figure 4.** Representative polar maps generated by RRG-SPECT and CZT-SPECT imaging in a CHF patient (A) and a non-CHF patient (B). Polar maps of MIBI myocardial perfusion (left) and regional MBF (middle) are displayed, alongside quantitated mean MBF values in three coronary territories (right). Global resting MBF values of the non-CHF patient were 0.83 and 0.82 mL·min<sup>-1</sup>·g<sup>-1</sup> and of the non-CHF patient were 1.14 and 1.16 mL·min<sup>-1</sup>·g<sup>-1</sup> with RRG and CZT SPECT, respectively.

**Table 6.** Test-retest repeatability of resting MBF measured with RRG-SPECT and CZT-SPECT in 20 CHF patients and 20 non-CHF patients

Group	Mean resting MBF of RRG-SPECT and CZT-SPECT (mL·min <sup>-1</sup> ·g <sup>-1</sup> )	RPC (mL·min <sup>-1</sup> ·g <sup>-1</sup> )	%
CHF	0.72 ± 0.26	0.18	25.0
Non-CHF	1.14 ± 0.17	0.22	19.2

The dynamic scans were acquired by the same experienced technologist and the image processing was performed by the same experienced physician

RPC, repeatability coefficient; %, RPC/(mean of resting MBF) × 100%

reconstruction, i.e., attenuation, scatter, resolution recovery, partial volume effect, and noise reduction. Moreover, we applied corrections for left and right ventricular spillover of MIBI activity, flow-dependent MIBI extraction fraction, and patient-specific rate-pressure product in kinetic modeling. All these corrections have been shown to be important to enhance the accuracy of MBF measurements using <sup>99m</sup>Tc-labeled tracers.<sup>5,7</sup>

We compared MBF values quantitated by RRG-SPECT and CZT-SPECT cameras because, although, both systems have the capability of dynamic SPECT imaging, their designs are very different. The CZT-SPECT camera has energy and spatial resolution which both may infer more accurate measurements of MBF than with RRG-SPECT. However, implementation of full physical and other corrections, as done in the present study, resulted in comparable quantitative MBF measurements and therefore appear essential for SPECT MBF quantitation. In this comparative study, we purposely designed to use the same controlled 20 mCi MIBI dose for both dynamic SPECT imaging on both RRG-SPECT and CZT-SPECT cameras. In fact, it may be desirable to lower the dose to 1/3 for CZT-SPECT to still preserve the same performance since it demonstrated three times higher total counts and count rates than those of RRG-SPECT.

Thus far, two major kinetic models have been proposed and validated for <sup>99m</sup>Tc-labeled tracers.<sup>2,3,6-8</sup> The first one is the one-tissue compartment (two-compartment) kinetic model as 1 vascular volume for

spillover estimation and 2 transport coefficients (K1, k2) for uptake rate and washout rate. The second one is the net-retention model as single transport coefficient (K1) combined with partial volume and spillover corrections. However, none of them have been validated in patients with CHF due to ischemic cardiomyopathy. We observed activity concentration in large infarcted areas may often be largely contaminated by excessive spillover from the adjacent cardiac blood-pool. In the present analyses, we applied a constraint in the one-tissue compartment kinetic model by utilizing patient-specific k2 originally estimated from fitting a patient's global myocardial time-activity curve with the standard one-tissue kinetic model. The modification assumes homogeneous and constant washout of MIBI and with excessive spillover in a large infarcted area with substantively low or zero MIBI uptake in CHF patients. As shown in Figure 5, the myocardial time-activity curve over an infarcted area with spillover from cardiac blood-pool mimics the arterial input time-activity curve. The kinetic model with three parameters (FBV, K1, and k2) would erroneously fit high initial uptake and rapid washout from myocardium and overestimate both K1 and k2. In our experience, using a constraint of patient-specific k2 can force the model to fit FBV and K1 during the process of numerical optimization. Importantly, for an area with normal perfusion, using the kinetic model with either three free parameters (FBV, K1, and k2) or two free parameters (FBV, K1) with one constrained parameter (fixed k2) did not cause a difference in K1 value. Consequently, a one-tissue compartment kinetic

**Table 7.** Static summed resting myocardial perfusion score (SRS) and left ventricular function parameters in 20 CHF and 20 non-CHF patients measured using RRG-SPECT and CZT-SPECT

	RRG-SPECT		CZT-SPECT	
	CHF	Non-CHF	CHF	Non-CHF
SRS	28.3 ± 14.8* (3 to 40)	4.85 ± 3.37 (1 to 19)	27.3 ± 13.6* (6 to 42)	4.05 ± 3.79 (1 to 12 <sup>++</sup> )
LVEF (%)	29 ± 8* (16 to 45)	65 ± 10 (47 to 85)	27 ± 8* (6 to 42)	70 ± 9 (47 to 87)
ESV (mL)	142.6 ± 68.7* (38 to 292)	27.8 ± 14.2 (6 to 52)	150.1 ± 70.8* (47 to 310)	28.1 ± 14.5 (6 to 47)
EDV (mL)	194.1 ± 79.7* (65 to 366)	77.3 ± 21.8 (39 to 114)	204.8 ± 81* (82 to 376)	72.4 ± 22.8 (43 to 112)

Mean ± SD and range

SRS, summed rest scores; LVEF, left ventricular ejection fraction; ESV, end-systolic volume; EDV, end-diastolic volume  
\*Significantly different from the control group ( $P < 0.0001$ )

model with a patient-specific fixed k2 constraint, may be more appropriate for quantitation of SPECT MBF with MIBI tracer, particularly in CHF patients with large infarction.

We also observed excessive MIBI right ventricle spillover and overestimation of K1 and MBF in the septal region. Our corrective method analyzed the distribution of activity between septal and lateral walls. A threshold was then set to normalize activity in the septal wall region. The method assumes that a particular frame can be identified when MIBI activity enters the right ventricle but not yet has entered the left ventricle, therefore resulting in inhomogeneous activity distribution between these two walls. Thus, the method can reduce overestimation of K1 and MBF in the septal wall, while large right ventricle spillover occurred as shown in Figure. 6.

Previous studies have reported test-retest repeatability of PET and SPECT MBF quantitation.<sup>1,20,21</sup> Using the above described corrections and near-identical imaging protocols for dynamic imaging with RRG-SPECT and CZT-SPECT, we calculated a RPC of 0.18 mL·min<sup>-1</sup>·g<sup>-1</sup> for CHF patients and a RPC of 0.22 mL·min<sup>-1</sup>·g<sup>-1</sup> for non-CHF patients as 25% and 19.2% of their mean resting MBF, respectively. These RPC values are similar to those reported in comparative <sup>82</sup>Rb PET and MIBI SPECT.

### Study Limitations

An important limitation of our study is that no dynamic SPECT image acquisition was performed during stress. Although in the present study in two clinically different patient groups, while using the two different dynamic SPECT systems, MBF quantitation was not significantly different at rest, our findings need yet to be confirmed under vasodilator stress. Another limitation in our study can be observed is that the interobserver reproducibility for RRG-SPECT and CZT-SPECT cameras was not performed. A future study can be designed to address this limitation by quantitations for resting MBF, stress MBF, and myocardial flow reserve. In addition, similar rest MBF values between RRG-SPECT and CZT-SPECT cameras in our study do not necessarily indicate accuracies in respect of diagnostic results. In a future study, healthy normal volunteers should be inducted to develop lower limits of normal MBF using both dynamic SPECT systems, thus allowing for a more reliable diagnostic test interpretation.

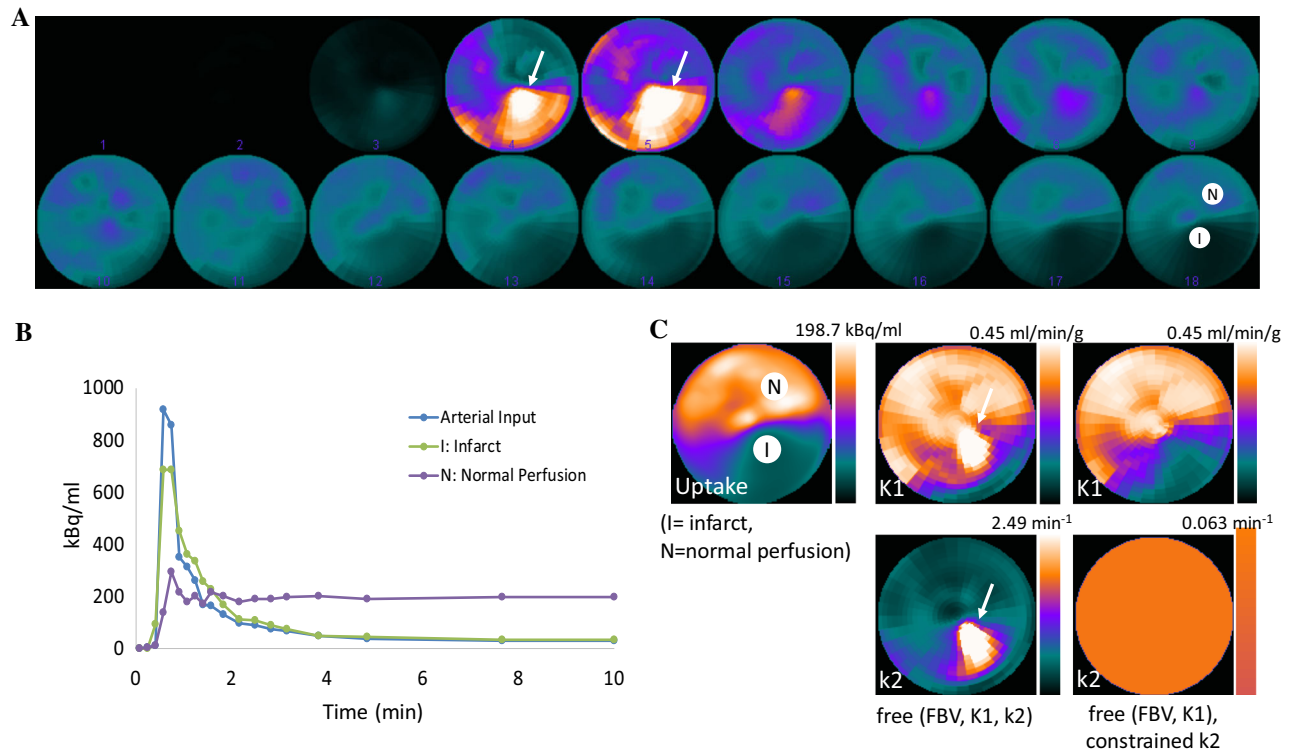


**Figure 5.** Example of a CHF patient with a large infarct in inferior and inferolateral walls from apex to base. (A) dynamic polar maps of myocardial uptake. (B) TACs of arterial input, of area with normal perfusion and infarct area. (C) Myocardial polar maps from the last frame (K1 and k2) with three free parameters (FBV, K1, and k2) and two free parameters (FBV and K1) and constrained k2. White arrows indicate excessive spillover from left ventricle. N, normal perfusion; I, infarct.

## CONCLUSION

Physical corrections along with other image corrections provide comparable MBF quantitations in both CHF and in non-CHF patients, regardless of which type of dynamic SPECT system is used.

## NEW KNOWLEDGE GAINED

From the data presented in the present study, readers may infer that by means of near-identical image acquisition parameters and the implementation of full image corrections during data processing, similar quantitative MBF measurements can be expected in the case of two state-of-the-art dynamic SPECT systems (RRG-SPECT and CZT-SPECT).

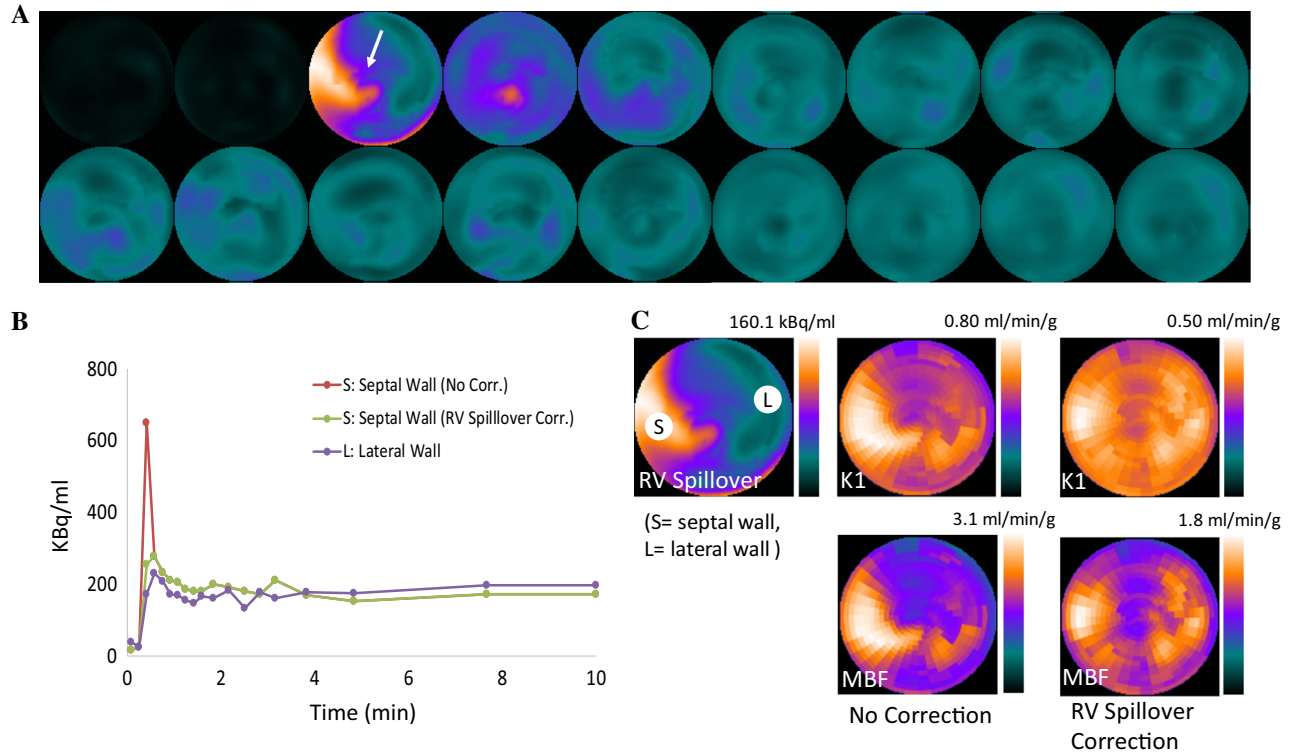


**Figure 6.** Example of RV spillover correction to reduce overestimated K1 and MBF in the septal wall. (A) Dynamic polar maps of myocardial uptake. (B) TACs of septal the wall with RV spillover, the septal wall with RV spillover correction, and the lateral wall. (C) effects of RV spillover correction on K1 and MBF in the septal wall region.

## Acknowledgements

This article was finalized under the auspices of the “Mentorship at Distance” committee of the Journal of Nuclear Cardiology. The authors gratefully acknowledge the editorial suggestions by Frans J. Th. Wackers, MD, PhD.

## Disclosure

BH, Scientific consultant, received support from Sinotaucloud Medical Technologies, Beijing, China. RM, LW, DW, MW, XS and WF declare that they have no conflict of interest.

## Ethical Approval

All procedures performed in studies involving human participants were in accordance with the ethical standards of the institutional and/or national research committee and with the 1964 Helsinki declaration and its later amendments or comparable ethical standards.

## References

1. Klein R, Hung GU, Wu TC, Huang WS, Li D, deKemp RA, et al. Feasibility and operator variability of myocardial blood flow and

- reserve measurements with  $^{99m}\text{Tc}$ -sestamibi quantitative dynamic SPECT/CT imaging. *J Nucl Cardiol* 2014;6:1075-88.
2. Hsu B, Chen FC, Wu TC, Huang WS, Hou PN, Chen CC, et al. Quantitation of myocardial blood flow and myocardial flow reserve with  $^{99m}\text{Tc}$ -sestamibi dynamic SPECT/CT to enhance detection of coronary artery disease. *Eur J Nucl Med Mol Imaging* 2014;41:2294-306.
3. Ben Bouallègue F, Roubille F, Lattuca B, Cung TT, Macia JC, Gervasoni R, et al. SPECT myocardial perfusion reserve in patients with multivessel coronary disease: correlation with angiographic findings and invasive fractional flow reserve measurements. *J Nucl Med* 2015;56:1712-7.
4. Nkoulou R, Fuchs TA, Pazhenkottil AP, Kuest SM, Ghadri JR, Stehli J, Fiechter M, Herzog BA, Gaemperli O, Buechel RR, Kaufmann PA. Absolute myocardial blood flow and flow reserve assessed by gated spect with cadmium-zinc-telluride detectors using  $^{99m}\text{Tc}$ -tetrofosmin: head-to-head comparison with  $^{13}\text{N}$ -ammonia PET. *J Nucl Med* 2016;57:1887-92.
5. Wang L, Wu D, Yang Y, Chen JJ, Lin CY, Hsu B, Fang W, Tang YD. Avoiding full corrections in dynamic SPECT images impacts the performance of SPECT myocardial blood flow quantitation. *J Nucl Cardiol* 2017;24:1332-46.
6. Hsu B, Hu LH, Yang BH, Chen LC, Chen YK, Ting CH, et al. SPECT myocardial blood flow quantitation toward clinical use: a comparative study with  $^{13}\text{N}$ -ammonia PET myocardial blood flow quantitation. *Eur J Nucl Med Mol Imaging* 2017;44:117-28.
7. Wells RG, Marvin B, Poirier M, Renaud J, deKemp RA, Ruddy TD. Optimization of SPECT measurement of myocardial blood

- flow with corrections for attenuation, motion, and blood binding compared with PET. *J Nucl Med* 2017;58:2013-9.
8. Agostini D, Roule V, Nganoa C, Roth N, Baavour R, Parienti JJ, Beygui F, Manrique A. First validation of myocardial flow reserve assessed by dynamic <sup>99m</sup>Tc-sestamibi CZT-SPECT camera: head to head comparison with <sup>15</sup>O-water PET and fractional flow reserve in patients with suspected coronary artery disease. The WATERDAY study. *Eur J Nucl Med Mol Imaging* 2018;45(7):1079-90.
  9. Ben-Haim S, Murthy VL, Breault C, Allie R, Sitek A, Roth N, et al. Quantification of myocardial perfusion reserve using dynamic SPECT imaging in humans: a feasibility study. *J Nucl Med* 2013;54:873-9.
  10. Bocher M, Blevis IM, Tsukerman L, Shrem Y, Kovalski G, Volokh L. A fast cardiac gamma camera with dynamic SPECT capabilities: design, system validation and future potential. *Eur J Nucl Med Mol Imaging* 2010;37:1887-902.
  11. Hudson HM, Larkin RS. Accelerated image reconstruction using ordered subsets of projection data. *IEEE Trans Med Imaging* 1994;13:601-9.
  12. Ichihara T, Ogawa K, Motomura N, Kubo A, Hashimoto S. Compton scatter compensation using the triple-energy window method for single- and dual-isotope SPECT. *J Nucl Med* 1993;34:2216-21.
  13. Bai C, Shao L, Da Silva AJ, Zhao Z. A generalized model for the conversion from CT numbers to linear attenuation coefficients. *IEEE Trans Nucl Sci* 2003;50:1510-5.
  14. Liu S, Farncombe T. Collimator-detector response compensation in quantitative SPECT reconstruction. *IEEE Nucl Sci Symp Conf Rec* 2007;5:3955-60.
  15. Soares EJ, Glick SJ, Hoppin JW. Noise characterization of block iterative reconstruction algorithms: II. Monte Carlo simulations. *IEEE Trans Med Imaging* 2005;24:112-21.
  16. Dutta J, Ahn S, Li Q. Quantitative statistical methods for image quality assessment. *Theranostics* 2013;3:741-56.
  17. Vanhove C, Andreyev A, Defrise M, Nuyts J, Bossuyt A. Resolution recovery in pinhole SPECT based on multi-ray projections: a phantom study. *Eur J Nucl Med Mol Imaging* 2007;34:170-80.
  18. Klein R, Beanlands RS, deKemp RA. Quantification of myocardial blood flow and flow reserve: technical aspects. *J Nucl Cardiol* 2010;17:555-70.
  19. Czernin J, Muller P, Chan S. Influence of age and hemodynamics on myocardial blood flow and flow reserve. *Circulation* 1993;88:62-9.
  20. Takahashi Y, Miyagawa M, Nishiyama Y, Ishimura H, Mochizuki T. Performance of a semiconductor SPECT system: comparison with a conventional Anger-type SPECT instrument. *Ann Nucl Med* 2013;27(1):11-6.
  21. Efseaff M, Klein R, Ziadi MC, Beanlands RS, deKemp RA. Short-term repeatability of resting myocardial blood flow measurements using rubidium-82 PET imaging. *J Nucl Cardiol* 2012;19(5):997-1006.

**Publisher's Note** Springer Nature remains neutral with regard to jurisdictional claims in published maps and institutional affiliations.